3

Hole Coupled Infrared Free-Electron Laser

Prazeres Rui
CLIO / Laboratoire de Chimie Physique
France

1. Introduction

Infrared FELs are used worldwide as user facilities. The FELs are especially efficient in infrared since they produce high power laser pulses, and are tunable across a large wavelength range, typically 1 to 2 decades, such as the CLIO mid-infrared laser facility which is covering from 3µm to 150 µm (Glotin et al., 1992; Prazeres et al., 2002; Ortega J.-M. et al., 2006). We are principally interested here in far infrared lasers. Several facilities are now operating in the world within this range:

- "CLIO", at Laboratoire de Chimie Physique, Orsay, France
- "FELIX", at FOM Institute, Nederland
- "FELBE", at Helmholtz-Zentrum Dresden-Rossendorf, Germany
- "FIR FEL", at IR-FEL Center, Tokyo University of Science, Japan
- "UCSB FEL", at University of California, Santa Barbara, U.S.A.

The amount of FEL optical gain which is required to achieve laser operation, i.e. to compensate the optical cavity losses, is easier to obtain in the infrared range than in visible or UV. Indeed, the FEL gain is strongly dependent on the electron beam energy γmc^2: in first approximation, the gain is proportional to $1/\gamma^3$. On the other hand, the FEL wavelength varies as $1/\gamma^2$. Therefore, large wavelength operation of the FEL requires low electron beam energy, which produces a larger amount of gain. Also, and this is a consequence of above comments, the requirements of quality (energy spread, emittance) of the electron beam are much less severe for infrared operation than for visible or shorter wavelength. This is why the X-ray FEL only have been developed recently, whereas the first FEL was operating in infrared (λ=3.4µm) in 1977 (Deacon et al., 1977). However, some other difficulties arise in infrared range: optical diffraction, absorption in materials or in air. Also, light detectors are less sensitive, cumbersome and more difficult to use - requiring liquid nitrogen, and liquid helium for far infrared. These difficulties have consequences on the design of an optical cavity for a far infrared FEL.

2. FEL optical cavity

The length of the optical cavity of a FEL must be rather large (a few meters) because it must include the undulator, magnetic dipoles and quadrupoles, electron beam deviation coils and various diagnostics. As a consequence, the Rayleigh length of the optical beam inside the cavity must be adapted, in order to avoid important optical beam divergence. The

transverse profile of laser must be less than the diameter of the cavity mirrors, and less than the aperture of all insertion devices, including the undulator vacuum chamber. It is important to keep the optical cavity losses at minimum value in order to get a maximum of laser power. The following calculation gives an approximate expression of the cut-off wavelength (upper limit) as a function of the geometrical configuration of the optical cavity. The Rayleigh length Z_R of a spherical cavity is (for a pair of identical mirrors):

$$Z_R = \frac{\pi . w_o^2}{\lambda} = \frac{1}{2}\sqrt{(d(2R_c - d)} \tag{1}$$

where d is the cavity length, R_c is the mirrors radius of curvature and w_o is the minimum of the waist $w(z) = w_o\sqrt{1 + (z/z_R)^2}$. The waist w_o is in the center (z=0) of the cavity. The cut-off wavelength λ_x can be defined by the condition where the laser mode hits the undulator vacuum chamber, i.e. when:

$$FWHM = 2.35.\left(\frac{W(L_w/2)}{2}\right) = b \tag{2}$$

where FWHM is the transverse size of the laser mode at the vacuum chamber extremity ($z=L_w/2$), L_w and b are respectively the length and the transverse aperture of the undulator vacuum chamber. This gives the cut-off wavelength λ_x:

$$\lambda_x = \frac{\pi . b^2}{Z_R} . \frac{0.72}{1 + \left(L_w / 2Z_R\right)^2} \tag{3}$$

For example, for CLIO with Z_R=1.2m, L_w=2m and b=14mm, we obtain $\lambda_x \cong 220\mu m$. In this case, the extremity of the vacuum chamber acts as a waveguide for the intracavity laser mode.

2.1 Hole coupling

Due to the lack of wide band multilayer transmitting mirrors or beam splitters, the only practical solution, to extract the laser power from the optical cavity, is to use a hole of a few millimeters in one mirror. In a preliminary configuration of the CLIO FEL in 1992 (Glotin et al., 1992), we used an intracavity Brewster plate to extract the laser power. Various materials was used: ZnSe from λ=3μm to 18μm, and KRS5 up to 40μm. However, this solution has two main consequences: the band-pass is limited due to absorption in the Brewster plate, and the variation of index of the plate creates a desynchronization of the FEL cavity length tuning according to wavelength.

Using a hole in the center of the output mirror avoids such problems, and this is presently the most commonly used system on FEL facilities (CLIO, FELIX, FELBE,...). Nevertheless, this is not a perfect solution, because it may alter the laser spot - as shown below. Moreover, the output coupling depends on wavelength. Indeed, the laser beam spot, on the output

mirror, increases with wavelength, thus the extraction rate T_x decreases with wavelength. The extraction rate T_x is the ratio between (1) the laser output energy (through the hole) and (2) the intracavity laser energy. Therefore, in practice it is useful to have, inside the vacuum of the cavity, a mechanical system that allows changing the output mirror, with several hole dimensions.

In first approximation, T_x should be proportional to the hole area, but in fact it is not the case because the intracavity laser profile is modified by the hole – it is a dynamic process in the cavity which leads to a steady state laser mode taking into account the perturbation due to the hole. The figure 1 shows a numerical simulation that has been performed with our code "MODES" (Prazeres & Billardon, 1992; Prazeres, 2001; Prazeres et al., 2005). It displays the output laser power at λ=20µm, as a function of the hole diameter, using the parameters of CLIO. For small holes, less than 2mm, the perturbation is negligible in the cavity, and the laser spot is not modified. But for a diameter of 3mm (point B), there is a jump of intracavity laser mode which creates a drop of the extraction rate T_x and consequently of the output power. This is due to a splitting of the laser profile on the output mirror (inside the cavity), as it is shown in the images on side of the curve. Such mode profile exhibits a minimum on the hole surface (at the center of the image), and reduces the extraction rate T_x.

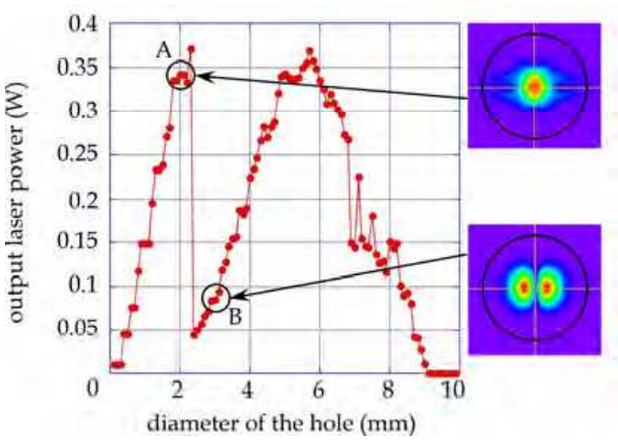

Fig. 1. Numerical simulation: output laser power vs. hole diameter (for CLIO data at λ=20µm). Images on side are the laser transverse profile inside the cavity, on output mirror. The black circles represent the mirror diameter of 38mm.

However, in practice, the tuning of the FEL operator is made so as to optimize the laser output power. It is a compromise between intracavity power and output coupling, and this procedure tends to select intracavity modes that are not necessarily centered on the hole. In this aim, the output mirror may be tilted by a few milliradians. This is shown in figure 2 which displays the output laser power as a function of mirror tilt on both axes (θ_x, θ_y). The point θ_x=θ_y=0 corresponds to the point B in figure 1, which the relevant laser profile exhibits a double spot in horizontal axis. Therefore, a horizontal tilt of the mirror allows the laser spot to fit upon the extraction hole. Indeed, the figure 2 shows that a horizontal tilt of 0.5mrd increases the laser power by a factor 5. In this case, as shown on the image on side, the laser spot fits better to the hole. This allows a better output coupling, and then a larger output power.

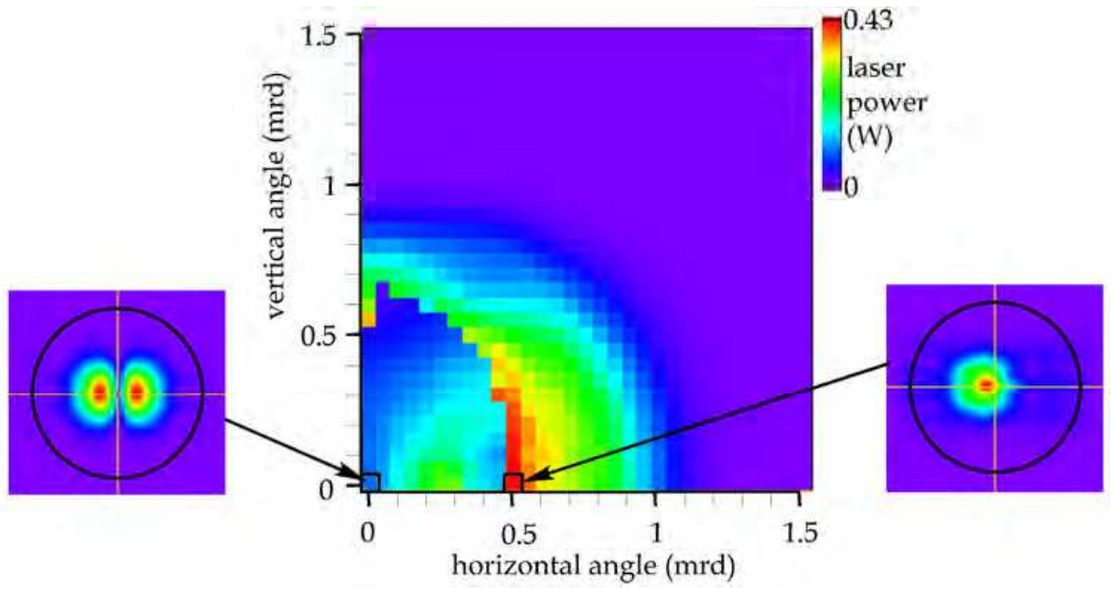

Fig. 2. Numerical simulation: laser power vs. angular tilt of the output mirror, at λ=20μm with a hole diameter of 3mm. Images on side are the laser transverse profile inside the cavity, on output mirror. The black circles represent the mirror diameter of 38mm.

As a consequence, it is not straightforward to calculate analytically the extraction rate T_x from the output coupling of a pure Gaussian mode. It is necessary to take into account the features of the intracavity laser mode. Also, when the intracavity laser profile is off-axis, or distorted, the output profile is strongly affected by the hole and does not keep the cylindrical symmetry of the system. These effects are analyzed here in section 5.

2.2 Undulator vacuum chamber

The transverse size of laser mode increases with wavelength, and beyond a certain limit it tends to undergo losses at the undulator vacuum chamber, which is generally the closer section of the FEL cavity. However, the transverse size of this chamber cannot be increased if one wants to maintain a sufficiently strong undulator magnetic field on-axis. Indeed, the upper limit of laser wavelength range corresponds to a maximum of magnetic field, which corresponds to the closer undulator gap. This determines the vacuum chamber transverse size along the magnetic field axis. On the other axis, there are no geometrical constraints because it is a free space - see fig.3. Therefore, the cross section of the vacuum chamber is, in principle, of rectangle shape with the shorter axis along magnetic field axis. However, due to pressure constraints upon the vacuum chamber, an elliptical shape offers a better rigidity. Such configuration is used on the CLIO FEL, as shown in figure 3. The minimum undulator gap is 18mm, and corresponds to an inner vacuum chamber size of 14mm on vertical axis. The inner size on horizontal axis is 35mm, it is large enough to avoid any diffraction problem. Note that in this chapter, we always consider a "usual configuration" of planar undulator, i.e. with magnetic field on vertical axis. Therefore, when speaking in this chapter about "horizontal walls" of the undulator vacuum chamber, these are always perpendicular to magnetic field, as shown in the example of figure 3.

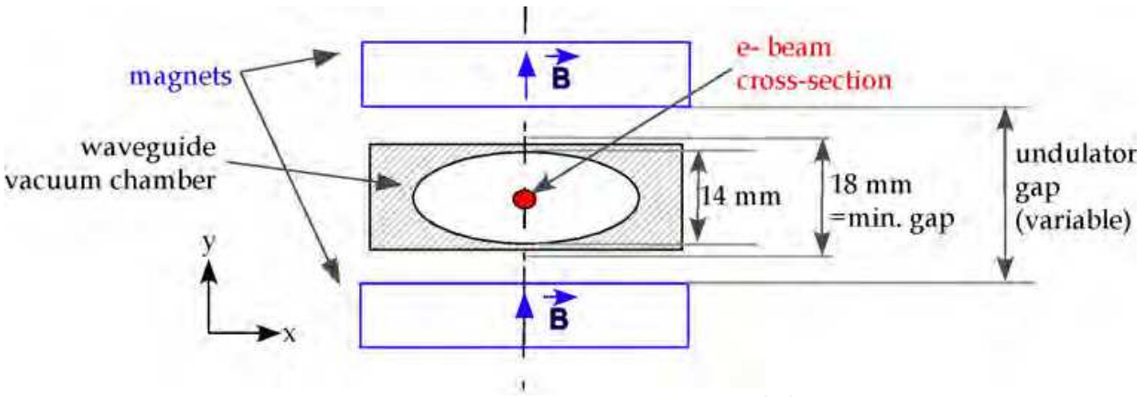

Fig. 3. Sectional drawing of the undulator vacuum chamber of the CLIO FEL

Some undulators are designed to be inside vacuum (Tanaka et al., 2005): the undulator gap can be as close as possible to the electron beam. This solution is used when a strong magnetic field is required, but the electron beam trajectory has to be very precise across the undulator in order to not hitting the magnets, which would create heavy damages.

The inner surface roughness of the undulator vacuum chamber is also an important parameter, because at large wavelength the laser mode may be guided by the horizontal chamber walls. Indeed, the horizontal walls are closer to the laser mode, whereas vertical walls are far enough to avoid any guiding effect. This is equivalent, in first approximation, to an infinite plate horizontal waveguide. This approximation is also valid in the case of an elliptical cross section waveguide, as shown in figure 3. Therefore, the inner surface of the vacuum chamber must be of mirror quality for infrared spectral range. As an example, the vacuum chamber of CLIO is done in extruded aluminium, which possesses a good conductivity and reflectivity. Now, if we consider a pure Gaussian laser mode propagating through such waveguide, we can have two borderline cases: (1) at short wavelength, the laser divergence in the vacuum chamber is small enough to avoid any clipping by the metallic walls, and no guiding occurs – it is equivalent to free space propagation ; and (2) at large wavelength, close to the cut-off λ_x in expression (3), the laser mode fills the vacuum chamber cross section, creating a guided propagation across the chamber. Between these two extreme cases, i.e. for intermediate wavelengths, the guiding effect may only partially occur, i.e. only on the extremities of the vacuum chamber. In this case, the simple model of infinite plate horizontal waveguide is fully applicable. This model is involved in our numerical code "MODES" (Prazeres & Billardon, 1992; Prazeres, 2001; Prazeres et al., 2005), which is used in this chapter to calculate the FEL features such as: cavity optical losses, output coupling, laser mode profile, laser power,...

2.3 Configuration of the optical cavity

Two main configurations are possible for the optical cavity of an infrared FEL: (1) the waveguide fills the whole length of the optical cavity, from upstream mirror to downstream mirror, or (2) the waveguide only fills the undulator section, the other parts of the cavity being in free-space propagation. The 1st type of cavity has been used in the UCSB FEL (University of California Santa Barbara [UCSB], Center for Terahertz Science and Technology): the waveguide covers from upstream cavity mirror up to downstream mirror.

In this case, the waveguide cross section is rectangular, and both cavity mirrors are of cylindrical type: the mirrors are flat in vertical plane because of the guiding effect, and concave in horizontal plane because of the free-space propagation - we are here in the approximation of infinite plate waveguide. The 2nd type of cavity, that we can nominate "partially guided", is used on other FELs such as CLIO. The figure 4 represents a layout of the optical cavity of CLIO. In this case, both cavity mirrors are in free-space propagation, and are of concave type. There is also an example of "hybrid configuration", on the ELBE FEL (Helmholtz-Zentrum Dresden-Rossendorf [HZDR]), where the upstream cylindrical mirror is in contact with the waveguide, whereas the concave downstream mirror is in free-space.

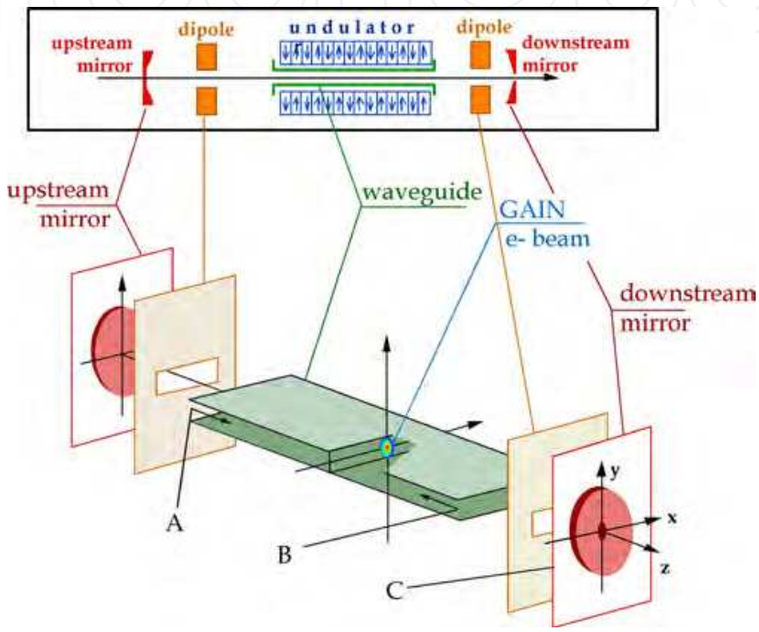

Fig. 4. Schematic layout of the CLIO Free-Electron Laser optical cavity

2.4 Radius of curvature of the cavity mirrors

When the laser wavelength is far from the cut-off λ_x in expression (3), the influence of the waveguide is negligible and a pair of spherical mirrors can be used for the cavity (R_X=R_Y). But for the "partially guided cavity" configuration, and at large wavelength, i.e. of the order of the cut-off wavelength λ_x, the waveguide section modifies strongly the laser mode. In this case, toroidal mirrors are more adapted for the cavity. The horizontal radius of curvature R_X is the same as for a free-space cavity, for both mirrors, because it corresponds to a free-space propagation. But for vertical axis, the calculations have shown (Prazeres et al., 2002) that it is necessary to focus the laser beam on the waveguide entrance. In this aim, the vertical radius of curvature R_Y must be approximately equal to the distance between the mirror and the waveguide entrance, for both mirrors. This is well described in the numerical simulation, in figure 5, using the codes "MODES" with parameters of CLIO. It shows, at various wavelengths, the laser power as a function of the vertical radius of curvature of both mirrors R_{1Y} and R_{2Y}, where R_1 and R_2 are respectively upstream and downstream mirrors. We have R_{1X}=3m and R_{2X}=2.5m for horizontal axis. The "S" labeled square dots corresponds to a pair of spherical mirrors: R_{1X}=R_{1Y} and R_{2X}=R_{2Y}.

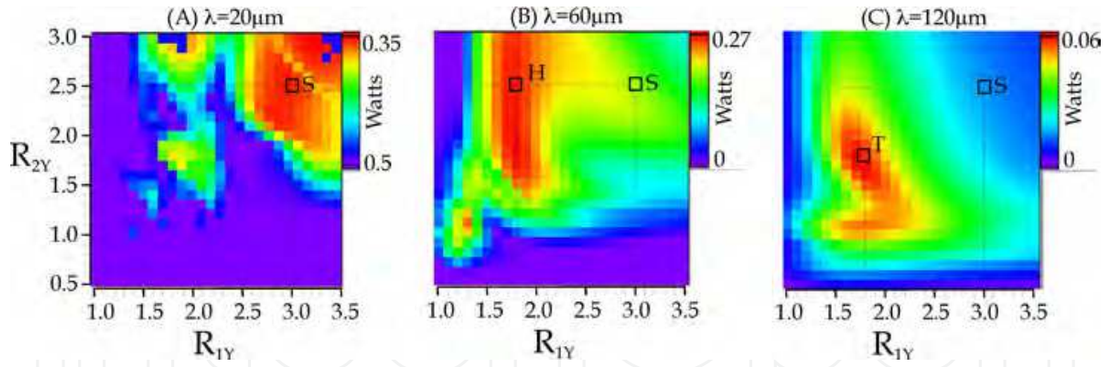

Fig. 5. Numerical simulation at (A) λ=20μm, (B) λ=60μm and (C) λ=120μm: laser power vs. radius of curvature in vertical plane, of both cavity mirrors. Abscissa corresponds to upstream mirror, and ordinate to downstream mirror.

The best configuration at λ=120μm is a pair of toroidal mirrors, with R_{1Y}=R_{2Y}=1.8m in vertical, and R_{1X}=3m and R_{2X}=2.5m in horizontal. It is represented by a "T" labeled dot. However, in practice, when using a pair of toroidal mirrors, the main difficulty appears during the procedure of alignment of the cavity: when using an HeNe laser, the red spot is deformed and spread out in vertical plane. This makes the alignment much more difficult as when using spherical mirrors. A good compromise is to use a "hybrid cavity", at least for the intermediate wavelength range: a toroidal upstream mirror, and a spherical downstream mirror that has a hole in center for output coupling. The "hybrid cavity" is represented by a "H" labeled dot on the figure, and it corresponds to the optimum power at λ=60μm. Consequently, and as spoken above, a mechanical system in vacuum for changing the output mirror may be very useful to swap rapidly the cavity mirrors. Such system is used in several FELs: CLIO, FELIX,...

3. Shift of undulator resonance in the waveguide

The waveguide, which is used in the undulator section, has an influence on the FEL process. Indeed, the phase velocity, inside the waveguide, is dependant on the eigenmode number, and then the resonant condition of the undulator is modified (Nam et al., 2000). This resonant condition requires that: during the travel of an electron through a period λ_o of the undulator, the radiation, which is produced by the electron, crosses the same distance plus one wave period λ. In free-space, this condition can be written:

$$v_z t = l_o \text{ and } ct = l_o + l \tag{4}$$

where v_z is the longitudinal velocity of the electron in the undulator. This is equivalent to:

$$\omega = c\beta_z (k_o + k) \tag{5}$$

where β_z=v_z/c is the normalised longitudinal velocity of the electron, k_o=2π/λ_o is the undulator wavenumber and and k=ω/c is the wavenumber. This gives the resonant frequency ω_R in free-space:

$$\omega_R = k_o \frac{c\beta_z}{1-\beta_z} \tag{6}$$

corresponding to the well known expression of resonant wavelength in free-space:

$$\lambda_R = \lambda_o \frac{1-\beta_z}{\beta_z} = \frac{\lambda_o}{2\gamma^2}\left(1+\frac{K^2}{2}\right) \tag{7}$$

where K is the undulator parameter and γ is the normalized electron energy.

In the waveguide (Bonifacio & De Salvo Souza, 1986), the resonant condition is written:

$$\omega = c\beta_z (k_o + k_{//}) \tag{8}$$

and the dispersion relation is:

$$\omega = c\sqrt{k_\perp^2 + k_{//}^2} \tag{9}$$

The wavenumber $k = \sqrt{k_{//}^2 + k_\perp^2}$ is a combination of (1) the longitudinal wavenumber $k_{//}=\omega/v_\varphi$, where v_φ is the phase velocity in the waveguide, and of (2) the transverse wavenumber $k_\perp=q\pi/b$, where q is the eigenmode number and b is the waveguide aperture along vertical axis (in the infinite plane parallel configuration). From these two expressions, resonant condition and dispersion relation, we obtain (Nam et al., 2000) two solutions ω_1 and ω_2 corresponding to the resonant frequencies in the waveguide:

$$\omega_{1,2} = \frac{\omega_R}{1+\beta_z}\left(1 \pm \beta_z \sqrt{1-X}\right) \tag{10}$$

where ω_R is the resonant frequency in free-space, $X = \left(k_\perp / \beta_z \gamma_{//} k_o\right)^2$ is the waveguide parameter and $\gamma_{//} = 1/\sqrt{1-\beta_z^2}$ is the longitudinal normalized energy of the electrons.

The situation where X=0 corresponds to the free-space configuration. The upper frequency ω_1 is equal to the "standard" resonant frequency ω_R of the undulator, and the lower frequency $\omega_2 \cong ck_o/2$ corresponds to a backward wave with the resonant wavelength $\lambda_2 \cong 2\lambda_o$ in the centimeter spectral range.

When X increases, X>0, the two frequencies ω_1 and ω_2 are shifting, and are converging one towards each other. The extreme situation where X=1 corresponds to the "zero slippage condition", where the wave group velocity $v_g=c^2/v_\varphi$ equals the electron bunch longitudinal velocity v_z. In this case, both frequencies are merging into a single resonant frequency $\omega_1=\omega_2 \cong \omega_R/2$.

When considering the FEL spectral range $\lambda<100\mu m$, and using an overmoded waveguide with an aperture $b>1cm$, then the waveguide parameter X is close to zero: $X<<1$. Therefore, it is possible to make a first order linear approximation of the upper resonant frequency ω_1:

$$\omega_1(q) \cong \omega_R - \frac{q^2 \pi c \lambda_o}{4b^2} \tag{11}$$

corresponding to a resonant wavelength λ_1:

$$\lambda_1(q) \cong \lambda_R + \frac{\lambda_R^2 q^2 \lambda_o}{8b^2} \tag{12}$$

As an example, for CLIO, the cut-off wavelength of the waveguide is $\lambda_c=2b/q = 28mm$ for the first mode q=1. The wavelength is in the range: $5\mu m<\lambda<150\mu m$. The relative wavelength shift $(\lambda_1(q)-\lambda_R)/\lambda_R$ is shown in the table 1, as a function of the mode q, for different wavelengths.

$(\lambda_1(q)-\lambda_R)/\lambda_R$ (in %)	q=1	q=3	q=5
$\lambda_R = 50\mu m$	0.15 %	1.4 %	4 %
$\lambda_R = 100\mu m$	0.32%	3%	8%

Table 1. Percentage of shift of the undulator wavelength resonance

This shift has to be compared to the linewidth of the undulator radiation: $\Delta\lambda/\lambda_R \cong 1/N$, where N is the number of undulator periods. We have for CLIO $\Delta\lambda/\lambda_R = 2.5$ %, with N=40. Therefore, the wavelength shift of the resonance is negligible for the mode q=1, but is important for $q \geq 5$.

In principle, this may have an important consequence on the FEL gain. Indeed, the spectral range of the FEL gain is centred on the resonance wavelength λ_R and it is limited, in first approximation, to the resonance wavelength linewidth, which is of the order of $\Delta\lambda/\lambda_R \cong 1/N$. When a waveguide is present in the undulator section, the laser mode is a sum of eigenmodes, with their own resonant frequency $\lambda_1(q)$. Therefore, at large values of resonance shifts $\lambda_1(q)-\lambda_R > \Delta\lambda$, for the eigenmode q, no gain occurs. In other words, only the low order eigenmodes will be amplified by the FEL process because their wavelength remains inside the gain band-pass.

However, the coupling of eigenmodes compensates this effect of gain selection. Indeed, outside of the waveguide, i.e. in free space areas, the transverse distribution of laser amplitude A(x,y) is modified by the divergence and by the diffraction, and it is focused by the mirror on the waveguide entrance. This makes a recombination, a coupling of the eigenmodes, inside the waveguide, at each cavity round trip of the laser pulse. On the other hand, the FEL gain is limited, in transverse plane, to the electron beam cross-section. Therefore, only the central part of the eigenmode is amplified. This makes a distortion of the eigenmode profile, which creates a mode coupling and feeds the high order modes. As a consequence, and if we consider the worst case, where only the first mode q=1 is amplified, the mode coupling allows to share the benefice of the gain among the eigenmodes. In

addition, the high order modes, which are not interacting with the gain process, are not participating to the FEL gain saturation process. But these high order modes are still stored in the optical cavity, and are contributing to the laser pulse energy, although not contributing to the gain saturation process. The numerical simulations, which have been performed (Prazeres et al., 2009) using the CLIO FEL configuration, have shown that such effect of eigenmode selection by gain gives an error of less than 10% to 20% on the output power, and it does not change significantly the laser mode distribution.

4. "Spectral Gaps" phenomenon with a waveguided FEL

In a "partially guided" configuration, using in addition a hole coupling system, we have shown that a phenomenon called "spectral gaps" (Prazeres et al., 2009) may produce a strong drop of power at some wavelengths of the laser. This effect is always present, independently of FEL tunings, of hole coupling size or of cavity mirror radius of curvature. It is very inconvenient for users since holes are observed during the wavelength scan of the FEL. This effect is due to the influence of the waveguide in the optical cavity.

4.1 Power measurements (on CLIO)

As an example, we show here the measurements on the CLIO FEL. The figure 6 shows the output laser power of CLIO as a function of wavelength, for a 15 MeV electron beam. The points correspond to measurements, and the continuous line to a numerical simulation using the code "MODES". Spherical mirrors are used here for the cavity, with a hole of 2 mm for output coupling. These measurements have been recorded in a purged chamber in order to avoid laser absorption in air.

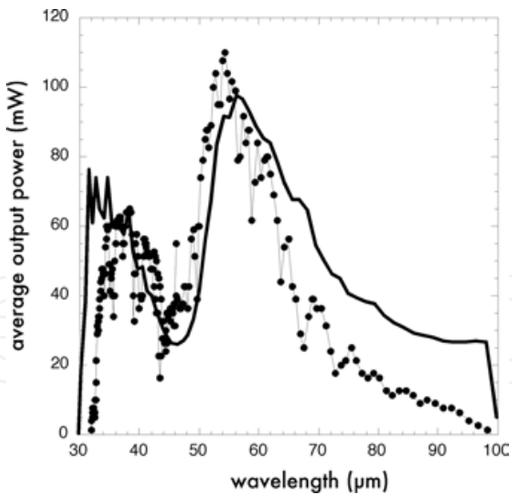

Fig. 6. Laser power vs. centroid wavelength, for spherical mirrors cavity, using hole coupling of 2mm (dotted line: measurement, continuous line: simulation)

A Spectral Gap appears at λ=45µm and corresponds to a power decrease by a factor of about 2. The simulation fits very well measurements, including the absolute value of the power, with a set of electron beam parameters: bunch charge Q=0.5nC, energy spread σ_γ/γ=0.5%, pulse length σ_z=4ps, emittance 150 π mm.mrd.

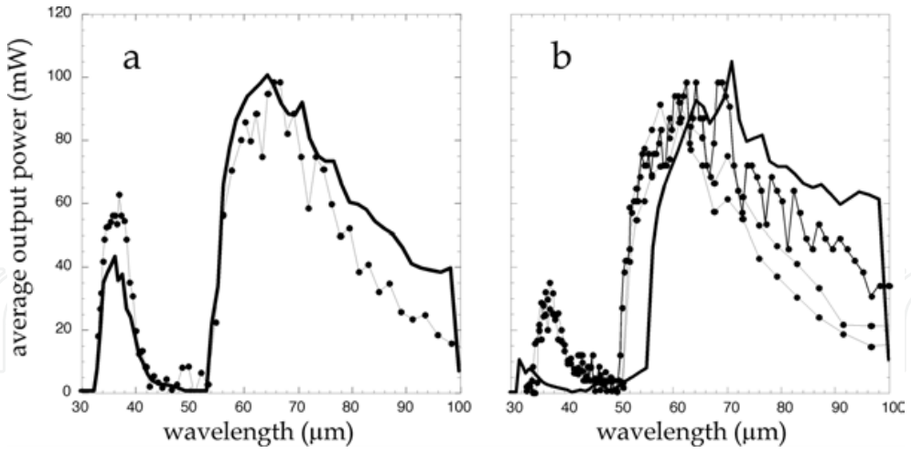

Fig. 7. Laser power vs. centroid wavelength, for hybrid cavity (a) and toroidal cavity (b), and using a hole coupling of 3mm (continuous line is a numerical simulation)

The figure 7a corresponds to another set of measurements, using a hybrid cavity (toroidal upstream mirror and spherical downstream mirror) with a 3mm hole coupling. The Spectral Gap is even more noticeable in this case. The figure 7b as been obtained with a full toroidal cavity, i.e. toroidal on both cavity mirrors. These measurements show that Spectral Gaps is an intrinsic effect, independent from the optical cavity configuration.

4.2 Simulation for a spherical cavity

In order to explain the Spectral Gap phenomenon, we used the numerical code "MODES" to compute the cavity losses L and the hole coupling extraction rate T_X as a function of wavelength, and the laser mode profile at various places in the optical cavity. The figures 8 and 9 show the results in the case of a spherical mirrors cavity, i.e. related to power variations of figure 6.

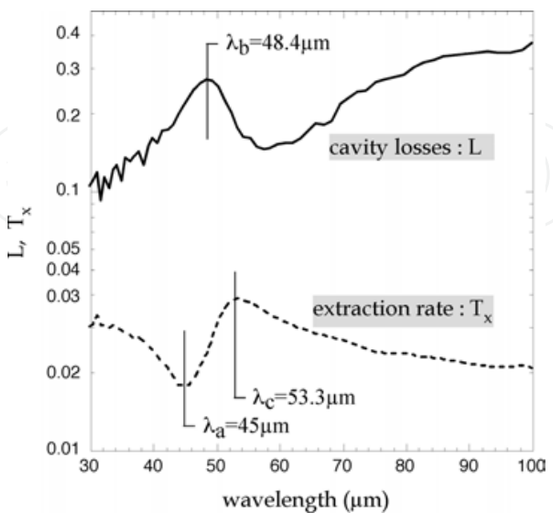

Fig. 8. Simulation of cavity losses L (continuous line) and hole coupling extraction rate T_X (dotted line) as a function of wavelength, for spherical cavity

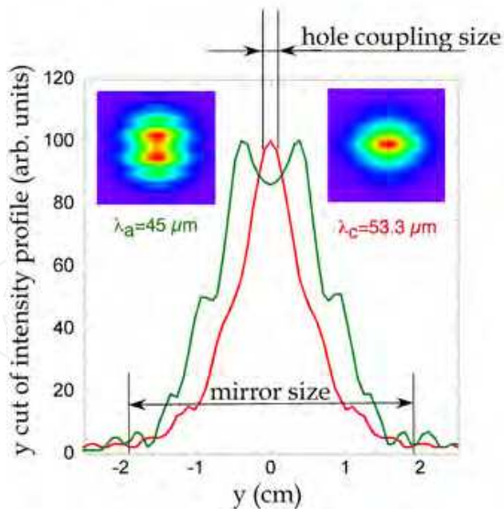

Fig. 9. Numerical simulation in the case of spherical cavity: laser mode transverse profiles on the output mirror, for 2 different wavelengths

The reason of the Spectral Gap is clearly visible here: the extraction rate T_X exhibits a minimum at wavelength λ_a=45µm - note that vertical axis is in log scale. The figure 9 displays the transverse profile of the laser mode, on the output mirror (point C in fig.4), for wavelengths λ_a=45µm and λ_c=53.3µm. At wavelength λ_a, the profile is wider and exhibits a small minimum of intensity in center, which accounts for the decrease of extraction rate T_X. This is a first explanation of the output power decrease at 45µm.

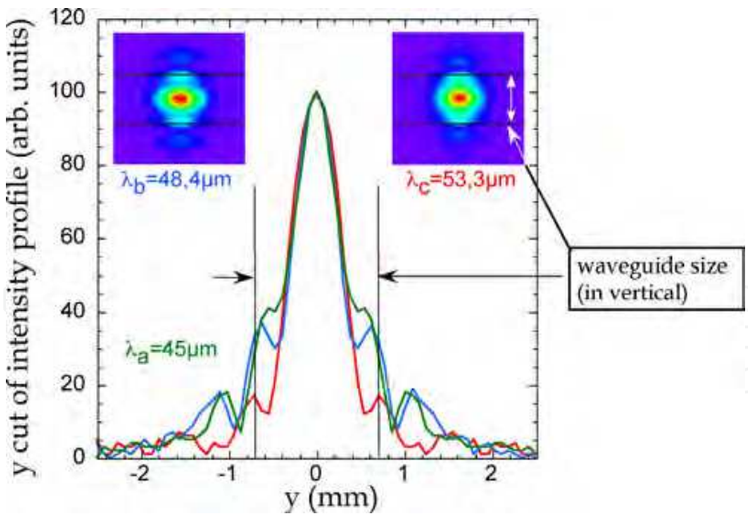

Fig. 10. Numerical simulation in the case of spherical cavity: laser mode transverse profiles on downstream waveguide entrance (point B in fig.4), for 3 different wavelengths

Indeed, this is not the only cause of Spectral Gaps: despite of the lower extraction rate, the cavity losses L are also maximum at wavelength λ_b=48.4µm - see figure 8. Note that mirror reflectivity is independent of wavelength, and Ohmic losses in the waveguide are negligible. A detailed analysis of the laser mode profile, at the waveguide entrance, is displayed in

figure 10. It shows that high losses, at wavelength λ_b, are due to a vertical broadening of the transverse size of laser mode, which does not fit the waveguide aperture. It occurs only in the vertical plane, where the laser mode is guided.

At λ_b=48.4µm, about 20% of laser energy is lost on each entrances of the waveguide. It represents only 8% at λ_b=53.3µm. These losses occur twice in a complete cavity round trip of the laser pulse. This explains the peak of losses in the curve of figure 8, which is also responsible for the Spectral Gap observed in figure 6.

4.3 Simulation for a toroidal cavity

As shown in figure 7b, the Spectral Gap phenomenon with a toroidal cavity is even stronger than in the case of spherical cavity (figure 6). The figure 11 shows the cavity losses L, and the hole coupling extraction rate T_X, as a function of wavelength, for a toroidal cavity.

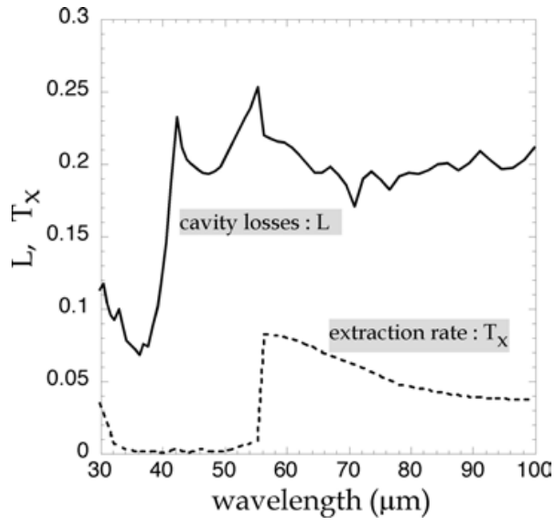

Fig. 11. Simulation, total cavity losses L and hole coupling extraction rate T_X as a function of wavelength, for toroidal cavity

The decreasing of the extraction rate T_X is much stronger here: there is a large range showing nearly zero extraction, between 32 and 55 µm. Also, within this range, the losses are varying strongly, and exhibit an important minimum at 37 µm. Such small losses are creating a large intracavity power P_{in}, as shown in figure 12 which displays both intracavity power P_{in} and output power P_{out}. The large value of P_{in} compensates partially the low extraction rate T_X, and leads to a significant output power P_{out} in the range 30-40µm. This effect is shown in simulations (fig.12), but it is even clearly observed in the measurements in figure 7b.

In real experimental conditions, a small misalignment of the cavity mirrors, or of the electron beam, may allow the intracavity power of the laser mode to be better out-coupled by the hole. This "default" is not taken into account in the simulations, and it could explain why the measured power overcomes the simulation in figure 7b in the range 30-40µm. This range corresponds to a critical situation where the intracavity power is large, whereas the extraction rate is reduced: the extracted power comes from this compromise.

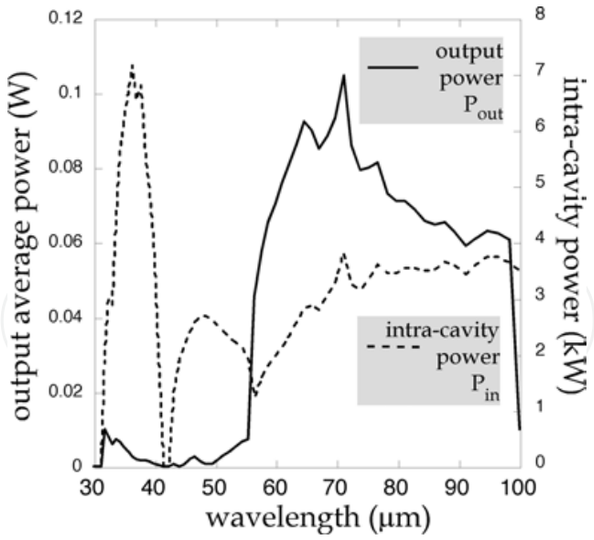

Fig. 12. Simulation, output power P_{out}, and intracavity power P_{in}, as a function of wavelength, for toroidal cavity.

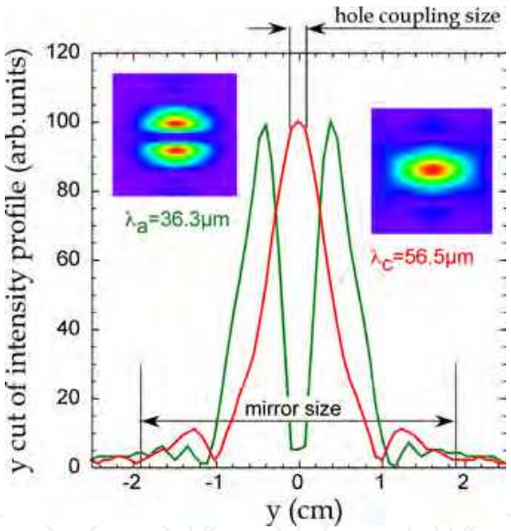

Fig. 13. Numerical simulation in the case of toroidal cavity: laser mode transverse profiles on the output mirror, for two different wavelengths.

The low extraction rate T_X for $\lambda < 55$ μm is explained by the image of laser mode on output mirror, displayed in figure 13: a double spot profile avoids the extraction hole close to λ=36μm. And the mode jumping, from 2 spots to 1 spot, at 56 μm, explains the sharp variation of T_X.

Also, the strong variations of cavity losses in figure 11 are due to variations of the mode profile at the waveguide entrance. Figure 14 displays the mode profiles at the downstream waveguide entrance (point B in fig.4), at 36μm and 55μm, corresponding respectively to minimum and maximum of cavity losses L. At λ=36.3 μm, the sum of optical losses, at both entrances, represents only 2.6%, which is rather low as compared to other wavelengths.

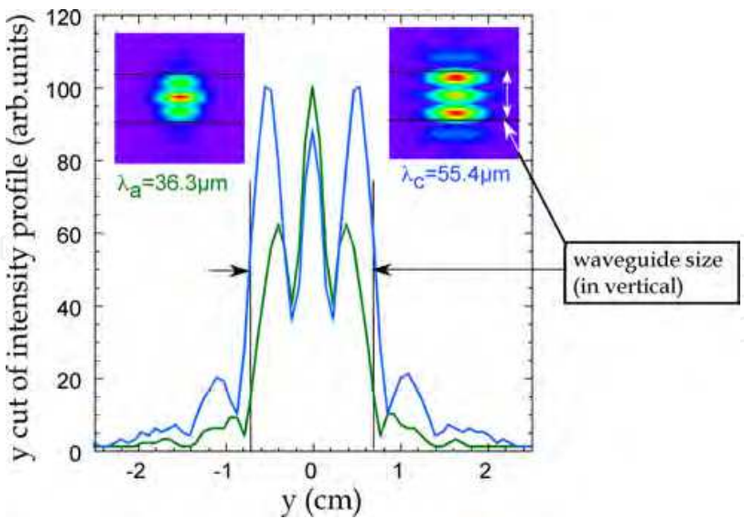

Fig. 14. Numerical simulation in the case of toroidal cavity: laser mode transverse profiles on downstream waveguide entrance, for two different wavelengths

As a conclusion, the explanation of Spectral Gap phenomenon is quite complex, because it is due to two effects: (1) a substantial increasing of cavity losses by clipping of the laser mode profile at the waveguide entrances, and (2) a minimum of the extraction rate T_X due to exotic transverse profiles on the hole coupling mirror. And both effects are strongly dependant on slight variations of the transverse mode profile. They are due to the presence of the waveguide. Indeed, we will see below that it is depending on the dimensions of the waveguide aperture.

4.4 Measurements on other FELs

The optical cavity of the FELIX infrared FEL (FOM Institute for Plasma Physics Rijnhuizen) is of same type as for CLIO, but with minor differences: the downstream cavity mirror is in contact with the waveguide, i.e. there is no free space between that mirror and the waveguide entrance. But there is a free space of 1.66 m in front of the upstream mirror. The distance between cavity mirrors is 6 meters, and the waveguide length is 4.34 m. The figure 15 shows a comparison between simulation, with "MODES" code, and measurement of the output power. Two measurements are displayed here: (1) for a perfect alignment of the cavity, and (2) for an alignment optimized at λ=35 μm. It shows that the Spectral Gap phenomenon exists on FELIX. The depth of Spectral Gaps may change with FEL alignment, but their positions remain identical.

The numerical simulation exhibits the two main Spectral Gaps, at 38 μm and 53 μm. A detailed simulation (Prazeres et al., 2009) makes a confirmation that the Spectral Gap is still due to two effects which are described above: (1) an increasing of optical losses by clipping into waveguide entrances, and (2) a reduction of the extraction rate T_X due to a split of the laser profile on the output mirror. The relevant laser profiles are shown in figure 15. The Spectral Gap occurs at wavelengths corresponding to a jump of laser mode into a complex shape.

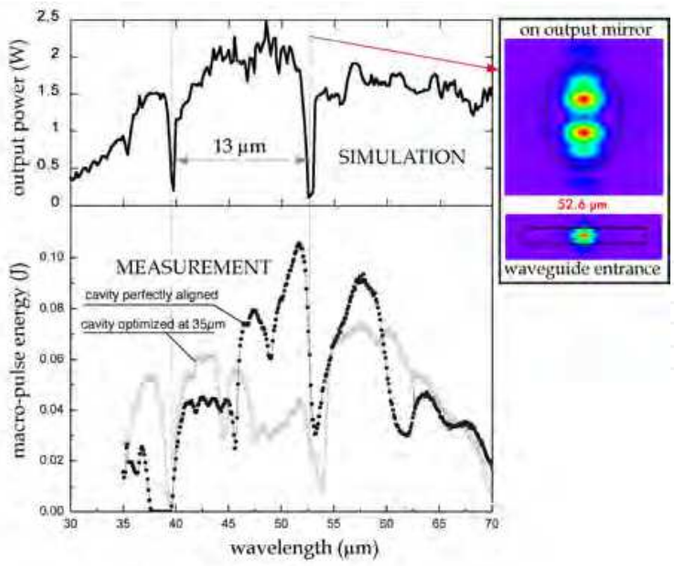

Fig. 15. Results for the FELIX infrared FEL

The configuration of the U100 FEL (Helmholtz-Zentrum Dresden-Rossendorf [HZDR], ELBE laboratory), is very similar to the FELIX FEL: the waveguide is in contact with downstream mirror. But the optical cavity is much larger, 11.5 meters long, and the waveguide also, 7.9 m. Figure 16 shows the result of a numerical simulation with "MODES" code. It displays the output power as a function of wavelength. Four Spectral Gaps are observed and they seem to be periodically spaced, with about a 7µm period. Unfortunately, the measurements of output power on ELBE are very lacunar, and they exhibit air absorption lines in the spectrum. A comparison with measurements is not available.

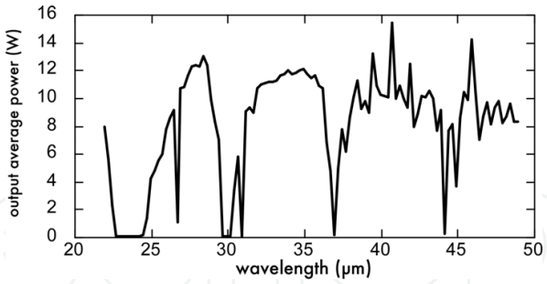

Fig. 16. Simulation of output power on the U100 FEL in ELBE, at 32MeV, with 2mm hole coupling

4.5 Analytical description of the Spectral Gaps

The Spectral Gaps (SG) phenomenon is due to a particular combination of eigenmodes TEq and TMq, produced in the waveguide, which creates a mode profile producing large losses or low extraction rate. These eigenmodes are only dependant on modes q because the waveguide is equivalent to infinite parallel plates. The figure 17 shows an example of the energy distribution of eigenmodes in the case of CLIO at λ=50 µm, corresponding to a mode profile which gives a two peaks structure on output mirror, as displayed in figure 13.

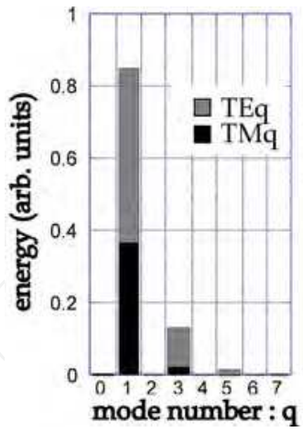

Fig. 17. Energy distribution of eigenmodes on TEq and TMq in the case of CLIO, with toroidal mirrors, at λ=50μm

Even modes are not present here, because they have a zero amplitude on axis and are not amplified by the electron beam that is centred on axis. This figure shows that the most important modes are q=1 and q=3.

It is likely that the phenomenon of SG is linked to the relative phase of the dominant cavity modes at the ends of the waveguide. Indeed, this phase will determine the diffraction losses at the entries of the waveguide and the mode structure at the extraction hole. Therefore, when sweeping the FEL wavelength, one expects that a phase difference of 2π in a cavity round trip will account for the wavelength difference between two successive SG.

The phase velocity in the waveguide for the mode q is:

$$v_\varphi = \frac{c}{\sqrt{1-\left(\lambda/\lambda_c\right)^2}} \cong c\left(1+\frac{\lambda^2 q^2}{8b^2}\right) \tag{13}$$

where $\lambda_c=2b/q$ is the cut-off wavelength, and b is the waveguide aperture in vertical axis. The approximation corresponds to an overmoded waveguide with $\lambda<<\lambda_c$. The propagation time of mode q, in a waveguide of length L_w, is $t_q=L/v_q$. The relevant dephasing of mode q is:

$$\Phi_q = \frac{2\pi}{T} t_q \cong \frac{2\pi L_w}{\lambda}\left(1-\frac{\lambda^2 q^2}{8b^2}\right) \tag{14}$$

the phase difference $\Delta\phi = \phi_1 - \phi_3$ between modes q=1 and q=3 is:

$$\Delta\Phi = \Phi_1 - \Phi_3 = \frac{2\pi L_w \lambda}{b^2} \tag{15}$$

and for a complete cavity round trip:

$$\Delta\Phi_{RT} = \Phi_1 - \Phi_3 = \frac{4\pi L_w \lambda}{b^2} \tag{16}$$

This calculation does not make any hypothesis on the absolute phase distribution of the modes. It only gives the phase shift between mode 1 and mode 3, for one cavity round trip. Now, when choosing λ corresponding to a SG, then the "next" SG in the FEL spectrum, at wavelength λ'> λ, must keep the same phase structure. This is the unique hypothesis that we do here: the phase structure is the same for all SGs (for a given FEL configuration, of course). Therefore, for:

$$\Delta\Phi_{RT}(\lambda') = \Delta\Phi_{RT}(\lambda) + 2\pi \tag{17}$$

one obtains:

$$\delta\lambda = \lambda' - \lambda = \frac{b^2}{2L_w} \tag{18}$$

where δλ is expected to be the wavelength difference (λ - λ') between two successive SG in the FEL power spectrum. Note that the 2π periodicity in expression (17) corresponds to a 4π periodicity when using a pair of higher modes q=3 and q=5. Therefore, as stated in the above hypothesis, the whole structure of modes TEq and TMq is kept constant between two consecutive SGs at λ and λ'.

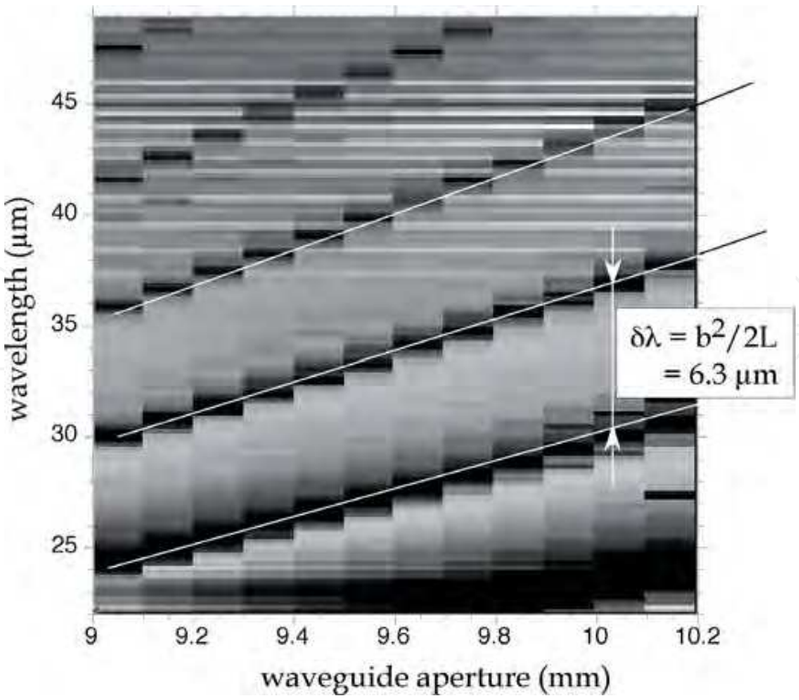

Fig. 18. Simulation – laser power vs. wavelength and waveguide aperture "b"

In order to check this simple analytical model, we show in figure 18 a simulation of FEL power as a function of wavelength, for various dimensions of waveguide aperture "b". The parameters used in this calculation correspond to the ELBE free-electron laser, which the geometrical configuration gives a short wavelength period $\delta\lambda$ for SG phenomenon.

The lines correspond to SGs, and the distance between two successive SG is 6.3 μm as predicted by the simple analytical expression (18) with b=1cm and L_w=7.92 m. Therefore, the simple model and the simulation agree very well, even if the available data do not allows to verify it experimentally.

Now for FELIX, the expression (18) gives $\delta\lambda$=11.5 μm, with b=1 cm and L_w=4.34 m. The simulation curve in figure 15 shows that the distance between two successive SG is $\delta\lambda$=13 μm, which is not far from analytical and experimental values.

For the case of CLIO, the expression (18) gives $\delta\lambda$=50 μm. The first SG in spectrum is measured at λ=45 to 50 μm. Therefore, the next SG should be observed close to λ=100 μm, which is not the case in the measurements. Indeed, we make the assumption here that such simple analytical model must be realistic when the wavelength period $\delta\lambda$ of SG is short as compared to the FEL wavelength full range. But a "large" period of $\delta\lambda$=50μm corresponds quite to the full spectral range, and the features the FEL are not constant between these two extreme points.

Nevertheless, the expression (18) provides an order of magnitude of the number N_{SG} of SGs in a given FEL spectral range (λ_{max}- λ_{min}):

$$N_{SG} \cong (\lambda_{max} - \lambda_{min}).2L_w / b^2 \tag{19}$$

Therefore, in the design of a far-infrared waveguide FEL, it is important to chose the waveguide geometry, with L_w and b, in order to reduce N_{SG} at minimum or at less than one.

5. Analysis of laser beam transverse profile

The hole coupling is a convenient system for laser extraction from the cavity. However, the intracavity optical mode is influenced by the hole, and this modifies the profile of the extracted light. The optimization of the FEL output power corresponds to a compromise between hole coupling extraction T_x and intracavity laser power P_{in}. Indeed, the "natural" tendency of the intracavity laser mode is to reduce the optical losses L, i.e. to create a mode with a minimum of hole coupling T_x, leading to a maximum intracavity power P_{in}. Whereas the desire of FEL user is to get a maximum of output power P_{out}=T_x*P_{in} which is proportional to the hole coupling T_x. Therefore, the machine parameters are adjusted in this aim. This compromise is mainly dependent on the relative values of 2 parameters: the laser wavelength and the extraction hole size. For "small" hole size, or large wavelength, the laser profile is not strongly affected, but the output coupling T_x is small. On the other hand, for "large" hole size, the intracavity laser profile tends to exhibit, on the output mirror, a minimum on Z axis which tends to reduce the output coupling T_x - see section 2.1. The better compromise is in between these two configurations. It gives a maximum of output FEL power P_{out}, but it still produces a distorted transverse profile of the output laser beam.

5.1 Laser profile measurements

In order to have a diagnostic of this effect, it would be interesting to have an image of the intracavity laser mode. But this is not always possible because of the mechanical configuration of the FEL cavity. Nevertheless, we have done measurements, on CLIO, of the laser profile outside of the cavity. These measurements have been done using a 2D infrared camera, which is placed outside of the optical cavity, and on the focal plane of a focusing mirror. The detector is a 2D matrix of pyroelectric detectors. The image, which is projected on the surface of detector, corresponds to the magnified image of the hole on output downstream mirror. The measured profile is shown on figure 19, for different wavelengths. At short wavelength ($\lambda < 10$ µm), as displayed in fig. 19a for λ=6.5µm, the profile always exhibits a typical "crescent moon" shape. Even when trying to modify all parameters of the FEL, we always obtain this typical profile. This shows that the intracavity laser mode is not centered on Z axis, and only one off-axis part of the profile is extracted by the hole. As the wavelength is increased, as shown in fig.19b for λ=17µm, the profile tends to fill the hole, as expected. The horizontal lines are due to diffraction in the laser beam line - outside of the cavity.

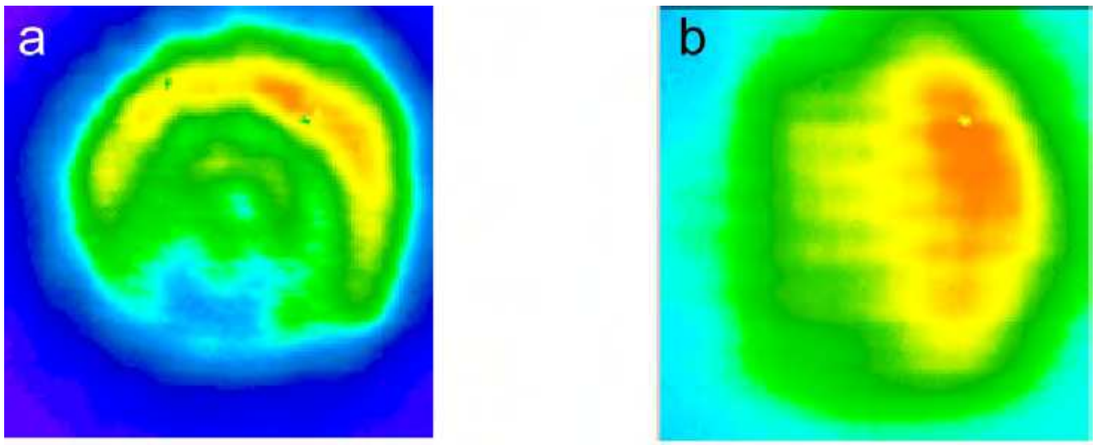

Fig. 19. Measurement of laser mode transverse profiles, in the experimental room, at λ =6.7 µm (a), and λ =17 µm (b)

Note that there is a competition, in the hole-coupled FEL configuration, between the hole extraction process and the optical gain process. The optical gain of the FEL is limited in space: it is limited along Z axis in the middle part of the undulator, and it is limited in (X,Y) plane by the electron beam cross-section, which RMS dimensions are close to 1 or 2mm. This forces the laser beam to stay on Z axis in the middle of the undulator. Whereas the hole on output mirror avoids that laser spot stays on Z axis at the extremity of the cavity. These two constraints force the laser beam to be misaligned in the cavity. As a consequence, the tuning of angular tilt of cavity mirrors, or the electron beam alignment in undulator section, have a strong influence on the intracavity laser mode, and they are crucial parameters for the output laser power P_{out}. As described here in section 2.1, a slight misalignment of the optical cavity breaks the axial symmetry of the laser mode and allows optimizing the output laser power P_{out}.

5.2 Numerical simulations

Indeed, numerical simulations have been performed with the "MODES" code, and they have shown that the output power may be increased by using a tilt θ on the output downstream mirror (while keeping upstream mirror at normal incidence). The relevant laser profile is displayed in figure 20, which shows a numerical simulation of the amplitude distribution A(x,y). It takes into account the same experimental conditions as for the measurements: it calculates the wave propagation along the optical beam line and through the focusing mirror up to the detector plane. The wavelengths are respectively λ=6.5μm (a) and λ=17μm (b). These profiles have been calculated using a tilt on output downstream mirror. This tilt is oriented of 45°, with $\theta_x=\theta_y$ =0.4mrd, in order to get θ=0.56mrd at 45° in the XY plane. These images may be compared to the image on figure 19, which have been measured in same conditions with the pyroelectric camera. The profile on fig.20a exhibits a "crescent moon" shape, which reproduces reasonably well the measurement. The profile on fig.20b is larger and fills the hole size, as shown in measurements on fig.19b.

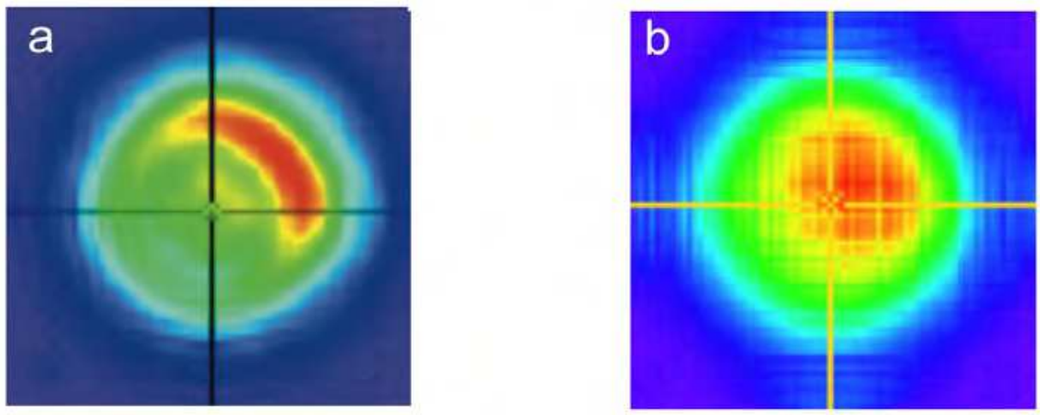

Fig. 20. Numerical simulation of laser mode transverse profile, calculated outside of cavity and within the experimental conditions, on the detector plane, at λ =6.7 μm (a), and λ =17 μm (b)

The figure 21 shows a simulation within same conditions, but it displays the profile inside of the cavity, on the output downstream mirror, at λ=6.7μm (a) and λ =17μm (b). The diameter of mirror (38mm) is represented by a circle, and the extraction hole (2mm) by a black dot in center. The laser profile exhibits, on fig.21a, a single spot, which is not centered on the hole. This explains the "crescent moon" shape of the extracted laser profile. At 17μm, the laser distibution is closer to the center of the hole, and this is sufficient to create a rather homogeneous output laser profile on fig.20b.

In order to show a comparison with on-axis alignment of the cavity, the figure 22 displays the result of the numerical simulation calculated for θ = 0, i.e. for normal incidence at the downstream mirror. In this case, the intracavity mode exhibits a double spot, in figure 22a, with a minimum on extraction hole and almost zero output power. In figure 22b, corresponding to the profile calculated outside of the cavity, on the detector plane, the mode also exhibts a double symmetrical spot. But in practice, it is not possible to observed such a laser profile, because of weakness of the power. This is another argument to say that the laser mode is never aligned on Z axis (Z axis being defined by the two centers of cavity mirrors).

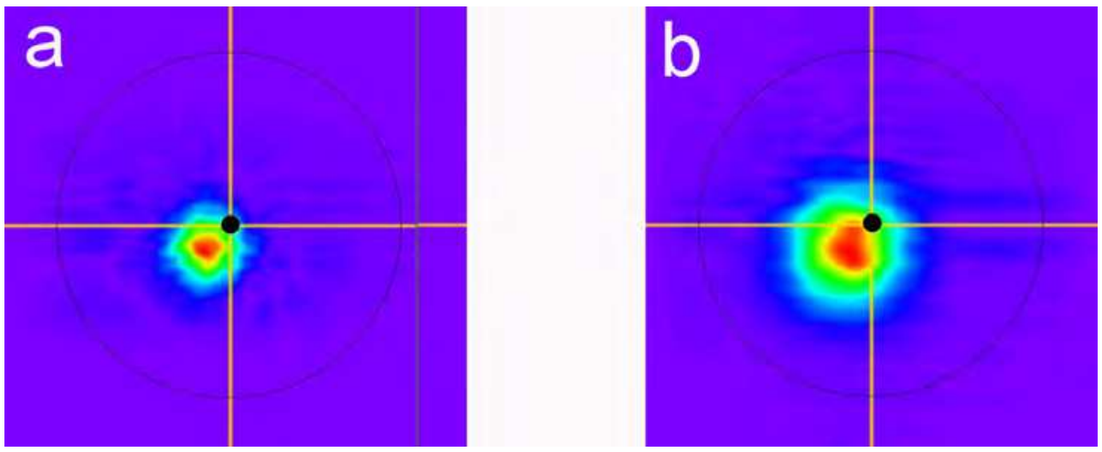

Fig. 21. Numerical simulation of laser mode profile inside of cavity and on downstream mirror, (a) at λ =6.7μm, (b) at λ =17μm

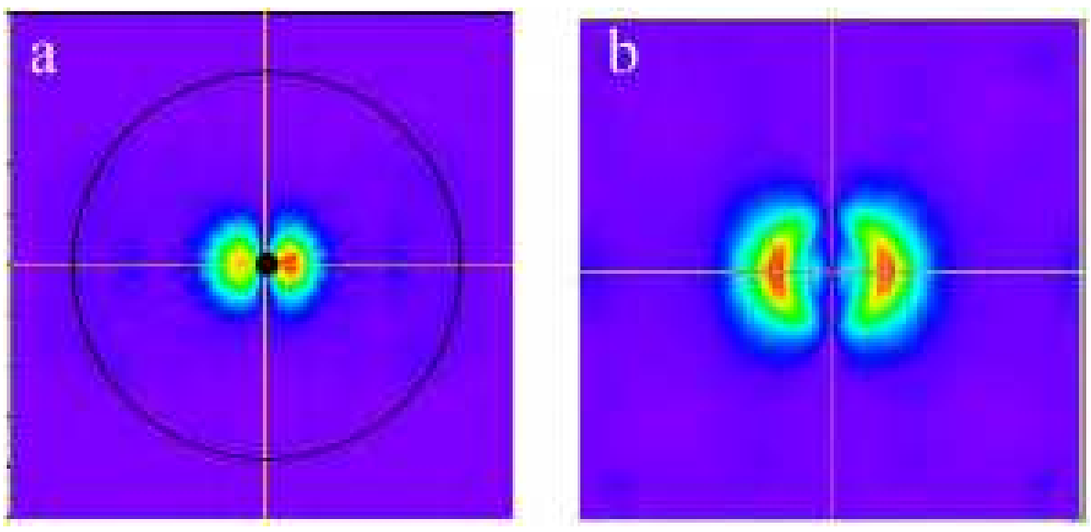

Fig. 22. Numerical simulation of laser mode profile, for λ=6.7μm, at normal incidence at the downstream mirror, (a) on cavity output mirror, (b) in experimental room

The competition phenomenon between the hole extraction process and the optical gain process, which is explained above, has been observed in the numerical simulations. The electron beam is centered on Z axis, and forces the laser mode to be aligned on the extraction hole (as an "automatic hole alignement process"). This effect is very important to get important output laser power, as it force the system to keep a large extraction rate T_x. In order to point out this effect, a numerical simulation has been done within same conditions as above, but using a flat electron beam profile, i.e. a large cross-section. This produces a uniform amplification of the laser cross-section, and avoids the effect of "automatic hole alignement". Within these (non realistic) conditions, the numerical simulation gave almost zero extraction rate T_x, and zero output power P_{out}, for any angular tilt θ of the downstream mirror. Therefore, if the laser beam is not pinched by the electron beam in the cavity, it always finds a position which avoids the hole. In other words, this shows that the small

electron beam cross-section forces the laser beam to pass through the hole. Whereas the "natural tendancy" of the laser mode would be to avoid the hole.

6. Conclusion

The far infrared is the most effective operating range for the free-electron lasers: large gain available, large output power. It represents also a most reasonable cost since using a "low" energy electron beam, and therefore it can be a rather compact device. However, some inconveniences require peculiar attention during the designing of such FEL. The optical diffraction imposes to use a waveguide in the optical cavity. Then, if the waveguide does not fill the whole cavity, a phenomenon of "Spectral Gaps" may occur, which creates a drop of power at some wavelengths within the FEL tuning range. In order to avoid these Spectral Gaps, the length of the waveguide has to be as short as possible, and its aperture must be as large as possible. The first constraint imposes a limit in the number of undulator periods, whereas the second one limits the maximum magnetic field on axis. A compromise has to be find with these parameters, as a function of the requirements for the FEL performances. On the other hand, the lack of wide band optics, in infrared, requires to use a hole coupling extraction in the optical cavity. However, this system produces generally an exotic laser transverse distribution ("crescent moon" shape) on the output laser spot. This effect may be very inconvenient for the users of the laser beam. It may be erased by reducing the hole dimension on the extraction mirror, but in this case the output laser power decreases.

The laser mode inside the optical cavity is generally not Gaussian because of the influence of the waveguide and of the hole coupling. It is a complex combination of divergence in free-space, guiding of eigenmode and diffraction by the hole. Therefore, a simple analytical model cannot be satisfying to describe the features of the laser mode. Contrariwise, a numerical code like "MODES" gives results that are in rather good agreement with the various measurements on CLIO, and even taking into account the absolute value of laser power.

7. Acknowledgment

We are thankful to Lex Van der Meer, and more generally to the FELIX free-electron laser group, for their contribution by sending us experimental data for the FEL

8. References

Bonifacio, R. & De Salvo Souza, L. (1986). Tuning and slippage optimization in a high-gain FEL with a waveguide. *Nucl. Instr. & Meth. in Physics Reaserch*, Vol.A276, pp. 394-398

Deacon, D.A.G.; Elias, L.R.; Madey, J.M.J; Ramian, G.J.; Schwettmann, H.A. & Smith, T.I. (1977). First Operation of a Free-Electron Laser. *Physics Review Letters,* Vol.38, pp. 892-894

Glotin, F.; Berset, J.M.; Chaput, R.; Kergosien, B.; Humbert, G.; Jaroszynski, D.; Ortega, J.M.; Prazeres, R.; Velghe, M. ; Bourdon, J.C.; Bernard, M.; Dehamme, M.; Garvey, T.; Mencik, M.; Mouton, B.; Omeich, M.; Rodier, J.; & Roudier P. (1992). First lasing of

the CLI0 FEL, *Proceedings of EPAC 1991 3rd European Particle Accelerator Conference*, pp. 620, Berlin, Germany, December 1991

NAM, S.K.; Yi, J. & KIM, K.B. (2000). *The small-signal gain in a waveguide free electron laser.* Journal of physical society, *Vol.37, No3, (September 2000), pp. 236-240*

Oepts, D. & van der Meer, A.F.G. (2010). Start-up and Radiation Characteristics of the FELIX Long Wavelength FEL in the Vicinity of a Tuning Gap. Proceedings of 32th International Free-Electron Laser Conference, pp. 323-327, Malmö, Sweden, August 23-27, 2010

Ortega, J.M.; Glotin, F.; Prazeres R. (2006). Extension in far-infrared of the CLIO free-electron laser. Proceedings of international Workshop on Infrared Microscopy and Spectroscopy with Accelerator-Based Sources (WIRMS 2005), Rathen, Germany, June 2005. Infrared Physics & Technology, Vol.49, pp. 133-138.

Prazeres, R; Glotin, F & Ortega, J.M. (2009). Analysis of periodic spectral gaps observed in the tuning range of free-electron lasers with a partial waveguide. *Physical Review Special Topics -Acceletors and Beams.* Vol.12, 0110701

Prazeres, R.; Glotin, F. & Ortega, J.M. (2005). Measurement and calculation of the "electron efficiency" on the "CLIO" free-electron laser. *European Physical Journal - Applied Physics*, Vol.29, pp. 223-230

Prazeres, R.; Glotin, F.; Rippon, C. & Ortega J.M. (2002). *Operation of the "CLIO" FEL at long wavelengths and study of partial guiding in the optical cavity.* Nucl. Instr. & Meth. in Physics Reaserch, *Vol.A483, pp. 245–249*

Prazeres R. (2001). A method of calculating the propagation of electromagnetic fields both in waveguides and in free space using the Fast Fourier Transform. *European Physical Journal - Applied Physics*, Vol.AP16, pp. 209-215

Prazeres, R. & Billardon, M. (1992). Numerical calculation of transverse optical modes for characterization of an optical cavity. *Nucl. Instr. & Meth. in Physics Reaserch*, Vol.A318, pp. 889-894

Tanaka, T.;Hara, T.; Tsuru, R.; Iwaki, D.; Marechal, X.; Bizen, T.; Seike, T. & Kitamura, H. (2005). In-Vacuum undulators, Proceedings of 27th International Free-Electron Laser Conference, *pp. 370-377, Stanford, USA, August 21-26, 2005*

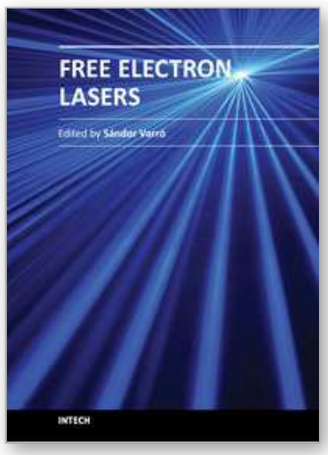

Free Electron Lasers

Edited by Dr. Sandor Varro

ISBN 978-953-51-0279-3
Hard cover, 250 pages
Publisher InTech
Published online 14, March, 2012
Published in print edition March, 2012

Free Electron Lasers consists of 10 chapters, which refer to fundamentals and design of various free electron laser systems, from the infrared to the xuv wavelength regimes. In addition to making a comparison with conventional lasers, a couple of special topics concerning near-field and cavity electrodynamics, compact and table-top arrangements and strong radiation induced exotic states of matter are analyzed as well. The control and diagnostics of such devices and radiation safety issues are also discussed. Free Electron Lasers provides a selection of research results on these special sources of radiation, concerning basic principles, applications and some interesting new ideas of current interest.

How to reference

In order to correctly reference this scholarly work, feel free to copy and paste the following:

Prazeres Rui (2012). Hole Coupled Infrared Free-Electron Laser, Free Electron Lasers, Dr. Sandor Varro (Ed.), ISBN: 978-953-51-0279-3, InTech, Available from: http://www.intechopen.com/books/free-electron-lasers/hole-coupled-infrared-free-electron-laser

INTECH
open science | open minds

InTech Europe
University Campus STeP Ri
Slavka Krautzeka 83/A
51000 Rijeka, Croatia
Phone: +385 (51) 770 447
Fax: +385 (51) 686 166
www.intechopen.com

InTech China
Unit 405, Office Block, Hotel Equatorial Shanghai
No.65, Yan An Road (West), Shanghai, 200040, China
中国上海市延安西路65号上海国际贵都大饭店办公楼405单元
Phone: +86-21-62489820
Fax: +86-21-62489821

IntechOpen